Cesium removal from solution using PAN-based potassium nickel hexacyanoferrate (II) composite spheres

Zhihui Du · Mingchun Jia · Xiaowei Wang

Abstract A polyacrylonitrile–potassium nickel hexacyanoferrates composite adsorbent was prepared to remove cesium ion in aqueous solution. The dual nozzle technique was applied to prepare a composite sphere. The physicochemical behavior of the ion exchanger was specified with different techniques including Fourier transform infrared spectroscopy, X-ray powder diffraction, specific surface analysis, scanning electron microscopy, and X-ray fluorescence spectroscopy analysis. The effects of contact time, solution initial pH, presence of various cations and initial cesium concentration on the adsorption was also investigated and the optimum conditions for separation of cesium were determined. In addition, adsorption kinetics and adsorption mechanism were studied by modeling the experimental data and related parameters were also evaluated, which showed that sorption data fitted to pseudo-second-order and film diffusion models. Adsorption isotherm in batch experiments showed that the sorption data were successfully fitted with Langmuir model. Finally the adsorption dynamic capacities of the synthesized composite in column experiments were evaluated at 139.925 and 119.539 mg/g for flow rate of 1 and 3 BV/min, respectively.

Keywords Cesium · Potassium nickel hexacyanoferrate (II) · Polyacrylonitrile · Sphere · Ion exchange · Adsorption

Z. Du (✉) · M. Jia · X. Wang
College of Power Engineering, Naval University of Engineering, Wuhan 430033, China
e-mail: 3072004003@163.com

Introduction

During the operation of nuclear power plants, reprocessing plants and research facilities, as well as the use of radioisotopes in industry and diagnostic medicine, a wide variety of liquid radioactive waste (LRW) have been produced. These wastes have to be treated to reduce the radioactivity to an acceptable level for discharge into the environment [1, 2]. All of these LRW types differ in chemical and radiochemical composition. The radiochemical composition changes significantly over time because of the decay of the short-lived radionuclides. In this process, the fraction of long-lived ^{137}Cs ($T_{1/2}$ = 32y), a major constituent of the fission products, increases continuously [3]. Consequently, many treatment schemes involve removing this isotope from the bulk waste in order to facilitate handling and storage at the repository.

Among various treatment schemes, insoluble hexacyanoferrates studied show very high affinity and selectivity for cesium ions [4]. But insoluble hexacyanoferrates exhibit a great variety of compositions and structures. Even with the same transition metal, different compositions and different structural arrangements may be observed, which depends on the method of preparation [5]. Meanwhile, insoluble hexacyanoferrates powders, if used as is, can cause operational problems such as pressure drop and filtration, which are not suitable for column application [6]. To avoid their disadvantages, insoluble hexacyanoferrates powders, as in most inorganic adsorbent powders, have to be palletized or immobilized to the other supporting materials. Among them, polyacrylonitrile (PAN) is reportedly one of the most favorable organic binders, due to its characteristic features such as excellent pelletizing property, good solubility for organic solvents, strong adhesive forces with inorganic materials and chemical stability [7, 8]. Several authors

reviewed the studies on PAN-based hexacyanoferrates composite adsorbent [9, 10]. Especially, Someda et al. [10] supported Cu, Zn hexacyanoferrates on PAN and applied them to the removal of cesium ions in aqueous solution. In spite of some successful results on the preparation of PAN-based hexacyanoferrates composite adsorbent, there are few papers on the preparation of spherical PAN-based potassium nickel hexacyanoferrates (KNiCF) composite adsorbent, and even fewer on its adsorption characteristic for cesium ions.

Therefore, this study was focused on the preparation of spherical PAN-KNiCF composite adsorbent and the evaluation of its adsorption behaviors for cesium ions.

Experimental

Reagents and apparatus

All the chemicals used in this investigation were of analytical grade purity and used without further purifications.

X-ray powder diffractometry was carried out using a model D/MAX-RB produced by RIGAKU Corporation and data were collected between 5° and 79.98° in 2θ. The infrared spectroscopy was recorded using a NICOLET 5700 FT-IR spectrophotometer from Thermo Electron Corporation. The specific surface analysis (BET) surface area and pore volume of studied adsorbents were determined using the nitrogen adsorption/desorption method by means of a surface area analyzer 3H-2000PS2. Scanning electron microscope (SEM) of the samples of the composite adsorbents synthesized was carried out using a model JSM-5610LV SEM produced by JEOL Ltd. The Axios advanced X-ray fluorescence unit is used to determine the amount of potassium, nickel and iron. The amount of Cs$^+$ was measured by an atomic adsorption spectrometer (AAS) model TAS-986F and finally the pH measurement was made with a pH-meter model PHS-3D.

Synthesis of composite adsorbent

Firstly the KNiCF was prepared by combination between $K_4[Fe(CN)_6]$ and $NiSO_4$ solution. The precipitate was filtered and then washed several times with deionized water and dried at 60°C for 48 h. The resulting granulates were ground to fine powder, and finally stored at room temperature.

A weighed amount of KNiCF which had been synthesized as above was measured in a weight ratio of 4:1 to PAN. The weighed amount of PAN was dissolved in solvent dimethylsulfoxide (DMSO) with gentle heat and continuous stirring, till a viscous solution was obtained. Then, the measured KNiCF was added to the mixture, and finally passed through inside the dual nozzle while the compressed air was ejected through the outside annulus of

the dual nozzle to adjust the size of the composite spheres [11]. The ejected composite spheres were then dropped in a deionized water bath and the PAN-KNiCF composite spheres were formed instantly to desired sphere size between 0.5 and 0.9 mm. These were washed with deionized water and dried at 60°C in an oven for 24 h. Finally, spherical PAN-KNiCF composite adsorbent consisting of approximately 80 wt% KNiCF loaded on a porous PAN support was synthesized.

Batch experiments

The adsorption experiments have been studied by batch technique. 0.02 g of the prepared composite adsorbent and 140 mL of the 20 mg/L cesium solution of desired pH were shaken with uniform speed using a thermostated shaker bath. pH of the adsorptive solutions was adjusted with the suitable quantity of NaOH and HCl. All experiments were carried out at 30 °C and pH 6.32 (±0.1). Before adding the adsorbent, an aliquot of the bulk solution was withdrawn for the measurement of the initial cesium concentration. For the evaluations of distribution coefficient (K_d) of cesium as a function of contact time, from 30 to 240 min time intervals were applied. At the end of each time interval, the cesium concentration of supernatant solutions was measured, and then K_d for adsorbed cesium on the composite was determined from the following equation:

$$K_d = \frac{C_0 - C}{C} \times \frac{V}{m} \tag{1}$$

where C_0 and C are the aqueous concentrations (mg/L) of the ion before and after treatment, m is the mass of adsorbent (g), V is the volume of waste solution (mL).

Also the same experimental conditions were applied in order to investigate the influence of solution initial pH, other cations (K^+, Na^+, NH_4^+, Ca^{2+} and Mg^{2+}) and initial cesium concentration on the distribution coefficient (K_d) of cesium. The adsorption isotherm experiments were conducted at the above experimental conditions by batch sorption procedure.

Column experiments

Column experiments were performed to investigate dynamic removal of cesium in aqueous solutions through adsorption. Total 0.5 g of PAN-KNiCF was packed in glass columns with a length of 410 mm and internal diameter of 6.5 mm. The cesium solution (20 mg/L) at pH 6.32 (±0.1) was pumped downward through the top of the column at a flow rate of 2.2 mL/min (1 BV/min) or 6.6 mL/min (3 BV/min).

Effluent samples were collected from the exit of the column at regular time intervals and then analyzed for residual cesium concentration using AAS.

Results and discussions

Characterization of the prepared composite adsorbents

Figure 1 shows XRD pattern for PAN-KNiCF, which clarifies the presence of some characteristic signals at different diffracting angels confirming the presence of crystal structure for PAN-KNiCF. In XRD pattern of PAN-KNiCF, a rather high crystallinity and narrow width of reflections which corresponds to the larger size of crystals are observed, and there are sharp peaks corresponding to $2\theta = 17.54°, 24.88°, 35.42°, 39.68°, 43.86°, 50.96°$ and $57.74°$.

The IR spectrum of PAN and PAN-KNiCF are recorded in Fig. 2. By comparing the data and IR spectrum of PAN and PAN-KNiCF, it was observed that the values of wavenumbers at the peak points of KCFC–PAN are close to those in KCFC, and their patterns almost match one another. In IR spectrum of PAN-KNiCF, the first peak around $3,408\ cm^{-1}$ is due to interstitial water and hydroxyl groups. The sharp and strong absorption peak at $2,095\ cm^{-1}$ corresponds to cyanide stretching region, and the peak at $1,612\ cm^{-1}$ is due to the deformation vibration of the free water molecules. Furthermore, the adsorption peak at 450–$600\ cm^{-1}$ region is due to the Fe–C stretching.

Nitrogen adsorption–desorption isotherm of PAN-KNiCF is shown in Fig. 3. Surface area of PAN-KNiCF is low, $29.63\ m^2/g$ calculated by BET method. Pore analysis of PAN-KNiCF was determined by BJH method based on nitrogen desorption isotherm. Cumulative pore volume and the average pore diameter of the adsorbent were determined as 0.16 mL/g and 26.43 nm, respectively.

The scanning electron microscopic photographs of PAN-KNiCF composite adsorbent are shown in Fig. 4. The images revealed that the particles are not homogeneous. The finely divided particles of the active components are embedded into the binding matrix. Many holes and cracks were observed on the surface of the adsorbent, which can cause fast kinetics of sorption on these adsorbents.

Using XRF spectroscopy, elements of potassium, nickel and iron were measured. The results achieved are shown in Table 1. According to Table 1 and the structure of hexacyanoferrate (II), the composition of KNiCF may be found as $K_{1.16}Ni_{1.37}[Fe(CN)_6]\cdot nH_2O$.
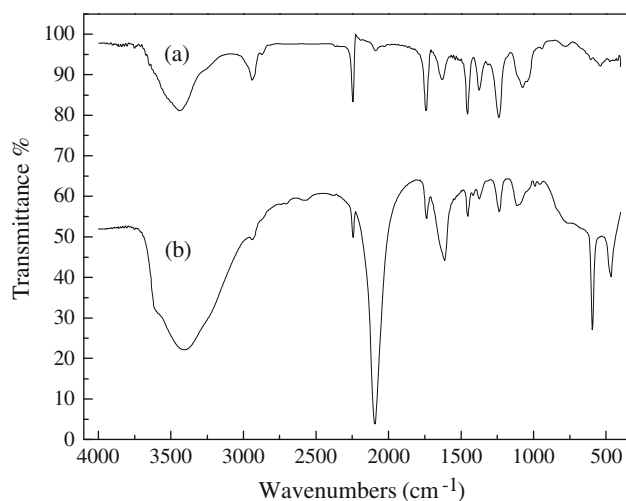
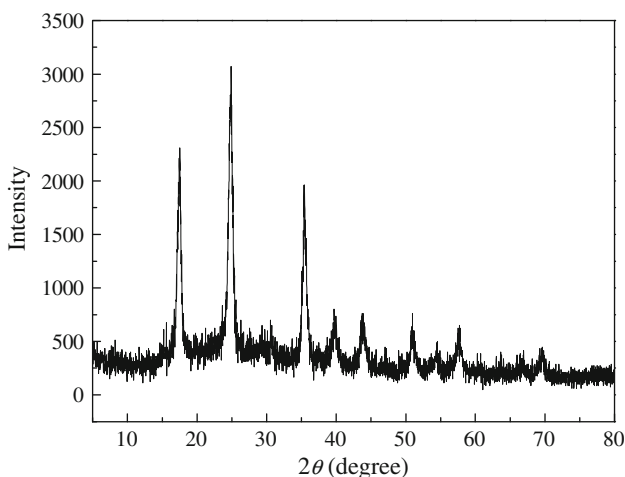**Fig. 2** IR spectrum of *a* PAN and *b* PAN-KNiCF

Fig. 1 XRD pattern of PAN-KNiCF
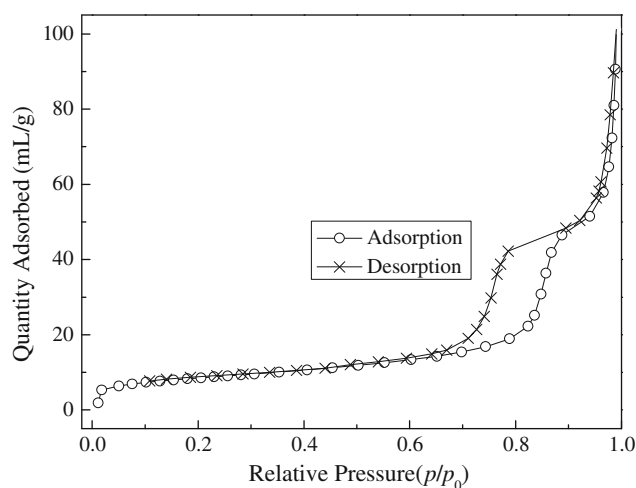
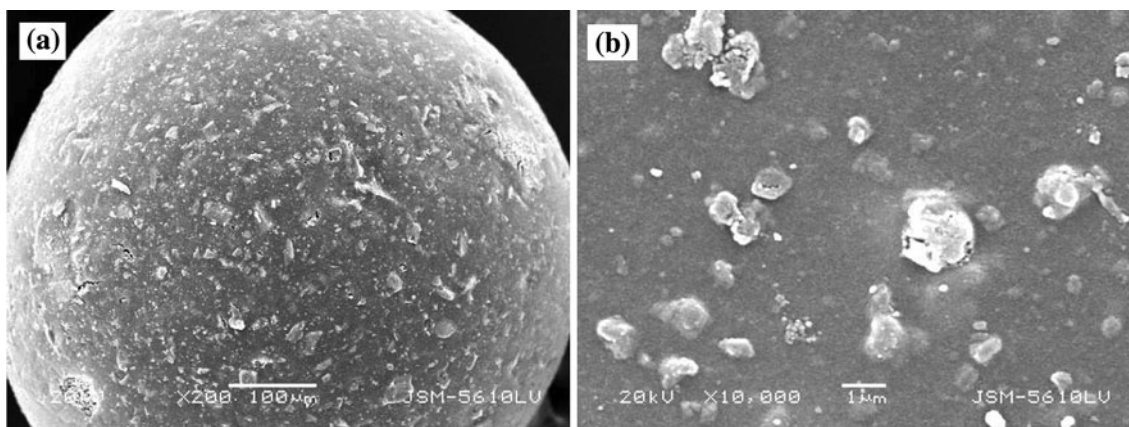**Fig. 3** Nitrogen adsorption–desorption isotherm of PAN-KNiCF

Fig. 4 **a**, **b** SEM photographs of PAN-KNiCF

Table 1 Analytical results of the prepared composite adsorbent

Element	Weight (%)
K	13.24
Fe	16.32
Ni	23.46

Batch experiments

Effect of contact time

The effect of contact time on cesium adsorption is given in Fig. 5, which shows that the adsorption rate soars with time increase, and equilibrium attained in about 24 h, showing the usual trend exhibited by ion exchangers: a fast initial adsorption followed by an almost constant value. In the subsequent experiments, the contact time of 24 h was selected for sorption equilibration of Cs^+ on PAN-KNiCF.
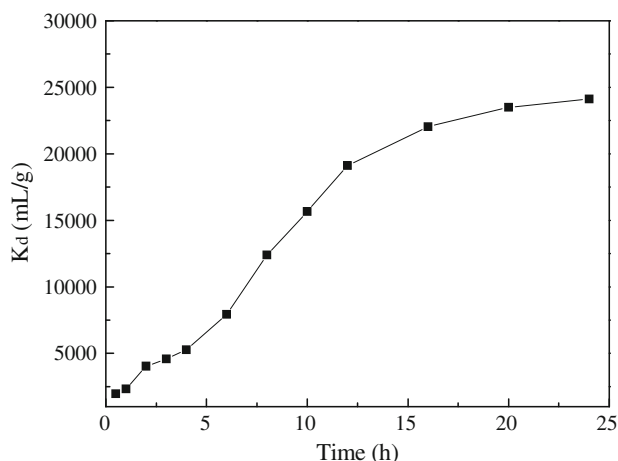
Effect of solution initial pH

The effect of pH on the sorption of Cs^+ from aqueous solutions using the prepared adsorbent was investigated over the pH range of 1.78–10.52. The results are shown in Fig. 6. The distribution coefficient of cesium on the PAN-KNiCF declines with increasing pH to a minimum value (pH 3.85) and then increases with further increase in pH. On the whole, low distribution coefficient in acidic environment was obtained, compared with alkali environment, which can be attributed to competition of H^+ with Cs^+ for the exchange sites in the adsorbent.

Effect of other cations

Various cations, often present in nuclear liquids, are likely to compete for the ion exchange sites in any sorbent and reduce the uptake efficiency of the sorbent. Hence, experiments were carried out to assess the adsorption behavior of
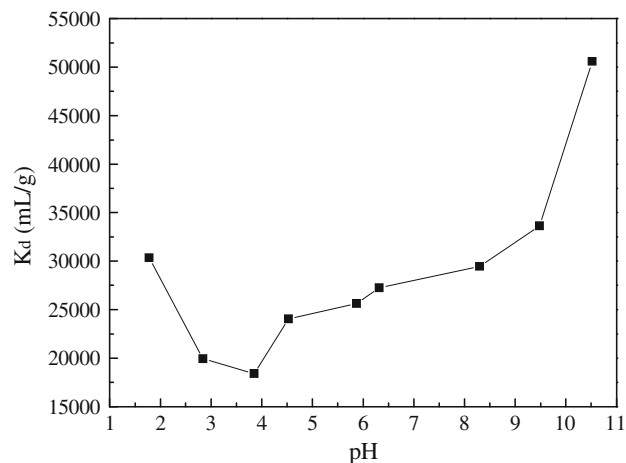

Fig. 5 Variation of distribution coefficient of cesium with contact time

Fig. 6 Variation of distribution coefficient of cesium with pH of the solution
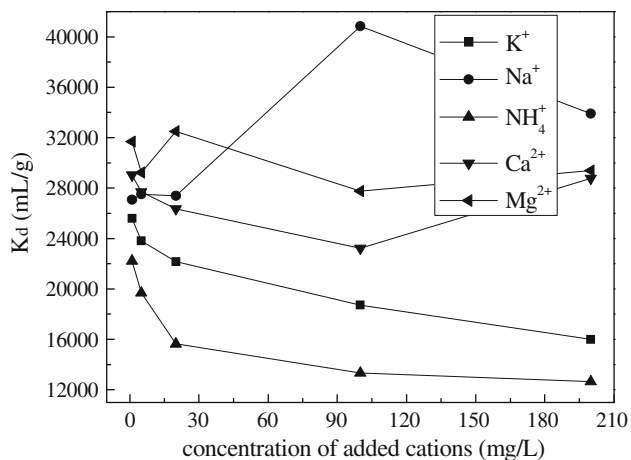
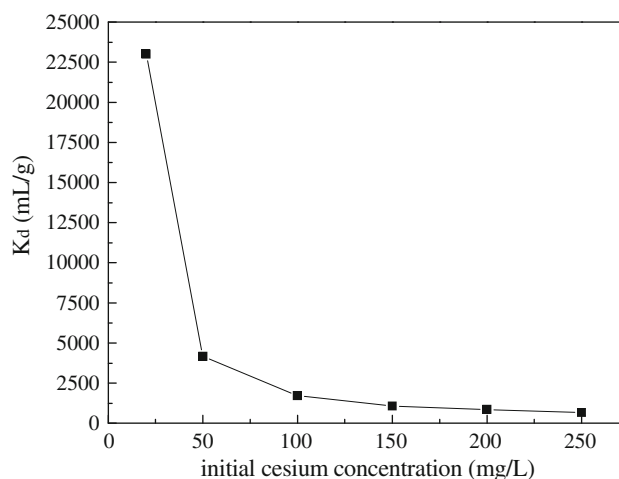Fig. 7 Variation of distribution coefficient of cesium with added cations

Fig. 8 Variation of distribution coefficient of cesium with initial cesium concentration

the prepared adsorbent for Cs^+ in presence and absence of K^+, Na^+, NH_4^+, Ca^{2+} and Mg^{2+}, while keeping constant the Cs^+ concentration (20 mg/L), pH (6.32 ± 0.1), and temperature (303 K). The concentration of the added cations varied from 1 to 200 mg/L. In absence of added cations, the value of K_d was 25,941 mL/g and the results under competition of added cations were returned in Fig. 7. The results indicate that the distribution coefficient of cesium decreased in the presence of K^+ and NH_4^+ and increased in presence of Na^+, Ca^{2+} and Mg^{2+}. Distribution coefficient of cesium decreased as the concentration of either K^+ or NH_4^+ increased and increased with increasing concentration of Na^+, but varied little as the concentration of Ca^{2+} or Mg^{2+} increased.

Effect of initial cesium concentration

Initial cesium concentration is an important factor that should be considered for effective adsorption. The distribution coefficient of cesium is presented in Fig. 8. The initial cesium concentration were increased from 20 to 250 mg/L, the distribution coefficient of cesium was rapidly decreased from 23,009 to 664 mL/g. This may be due to the saturation of active adsorption sites on PAN-KNiCF composite adsorbent.

Adsorption kinetics

The kinetics of adsorption describes the rate of cesium uptake on the PAN-KNiCF, which determines the equilibrium time. The kinetics of sorbate uptake is required for selecting optimum operating conditions for the full-scale batch process, and the kinetic parameters can reflect important information for designing and modeling the processes [12]. Thus, different kinetic models such as
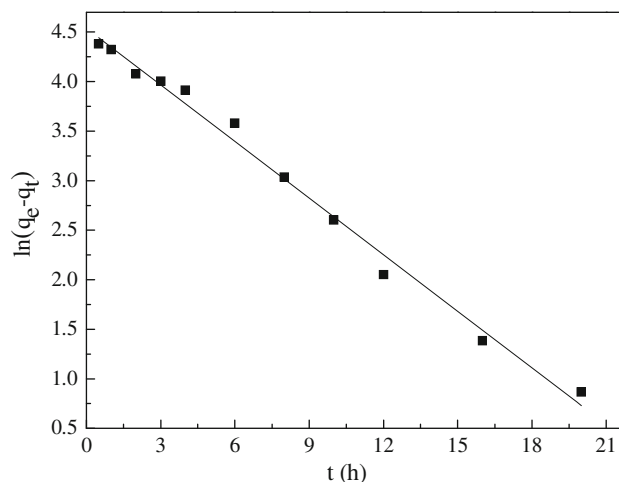

Fig. 9 Pseudo-first-order model plot for cesium adsorption on PAN-KNiCF

pseudo-first-order and pseudo-second-order models were used to analyze the kinetics of the sorption data.

Lagergren pseudo-first-order equation is the most popular kinetics equation and used only for the rapid initial phase. The pseudo-first-order equation is given by [13]

$$\ln (q_e - q_t) = \ln q_e - k_1 t \tag{2}$$

where q_t (mg/g) is the adsorption capacity at time t and k_1 (h^{-1}) is the first order rate constant. The value of k_1 can be obtained from the slope of the plot $\ln (q_e - q_t)$ versus t (Fig. 9). The estimated reaction rate and the correlation coefficient (R^2) values of fitting the first order rate model are reported in Table 2.

Pseudo-second-order equation may be expressed in the form [14]:

Table 2 Pseudo first and second order model parameters for the sorption of cesium

Pseudo-first-order model			Pseudo-second-order model				q_e experimental (mg/g)
q_e (mg/g)	k_1 (h^{-1})	R^2	q_e (mg/g)	k_2 (g/(mg h))	h (mg/(g h))	R^2	
93.652	0.191	0.990	124.224	0.00267	41.202	0.984	110.250
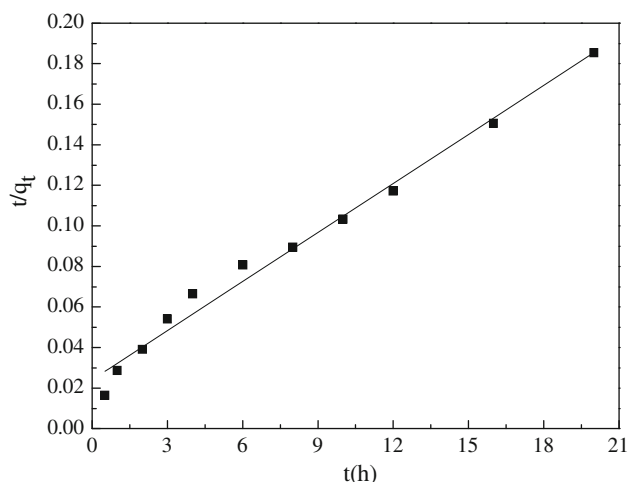
Fig. 10 Pseudo-second-order model plot for cesium adsorption on PAN-KNiCF

$$\frac{t}{q_t} = \frac{1}{k_2 q_e^2} + \frac{t}{q_e} \qquad (3)$$

where k_2 (g/(mg h)) is the second order rate constant. The second order rate constant can be used to calculate the initial sorption rate, at $t \to 0$ as follows [15]:

$$h = k_2 q_e^2 \qquad (4)$$

where h (mg/(g h)) is initial sorption rate. Figure 10 shows a plot of t/q_t against t and related parameters are shown in Table 2. From Table 2, it was noticed that correlation coefficient values of pseudo-first-order model was slightly higher than that of pseudo-second-order model. However, the q_e calculated value was found to be closer to q_e experimental value in pseudo-second-order kinetic model when compared to the pseudo-first-order kinetic model. Therefore, the sorption data fit pseudo-second-order model better.

Adsorption mechanism

From a mechanistic viewpoint, to interpret the experimental data, it is necessary to identify the steps involved during adsorption. It consists of the following three main steps [16]:

(1) Transport of the solute from bulk solution through liquid film to the adsorbent exterior surface (film diffusion);

(2) Transport of the sorbate within the pores of the adsorbent (intraparticle diffusion);

(3) Adsorption of the sorbate on the exterior surface of the adsorbent.

The last step is very rapid for most of the adsorption processes, and its corresponding resistance can be negligible. However, the rate limiting step is the slowest one. Hence, the rate limiting step might be determined between film and intraparticle diffusion, viz., film diffusion, or intraparticle diffusion, or both during the process of solid–liquid adsorption. The possibility of film or intraparticle diffusion was explored by using the Weber–Morris model [17]:

$$q_t = I + k_i t^{1/2} \qquad (5)$$

where k_i (mg/(g h$^{0.5}$)) is the intraparticle diffusion rate constant, t (h) is time and I (mg/g) is the intercept of the vertical axis and it gives information about the thickness of boundary layer. This intercept could be employed to examine the effect of diffusion mechanisms of the solute i.e. film and intraparticle diffusion. If the Weber–Morris plot of q_t versus $t^{0.5}$ gives a straight line trough the origin, $I = 0$, intraparticle diffusion is considered as the rate limiting step, while, at $I > 0$ both film and intraparticle diffusion are considered as rate limiting steps. The q_t values were plotted against $t^{0.5}$ as shown in Fig. 11. From Fig. 11, the straight line did not pass through the origin and this indicated that the intraparticle diffusion was not only the rate-controlling step.

The plot of q_t versus $t^{0.5}$ can also be divided into a multi-linearity correlation (Fig. 11), which indicates that three steps occur during adsorption process. For the first sharper portion, i.e. from 0 to 8 h, it is postulated that cesium was transported to the external surface of the adsorbent through film diffusion and its rate, $k_{i1} = 27.062$ mg/(g h$^{0.5}$) shows this adsorption process is very fast. The second portion is the relatively gradual adsorption stage where the intraparticle diffusion with $k_{i2} = 20.506$ mg/(g h$^{0.5}$) can be rate controlling. The third portion (after 12 h) $k_{i3} = 5.385$ mg/(g h$^{0.5}$) is the final equilibrium stage where the intraparticle diffusion starts to slow down due to the extremely low solute concentration in solution [18]. From the above analysis, it can be concluded that both film and intraparticle diffusion were simultaneously operating during the process of the adsorption of cesium on the PAN-KNiCF.
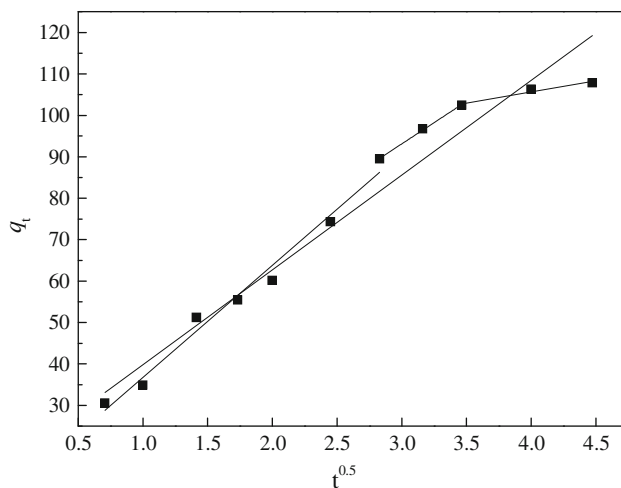
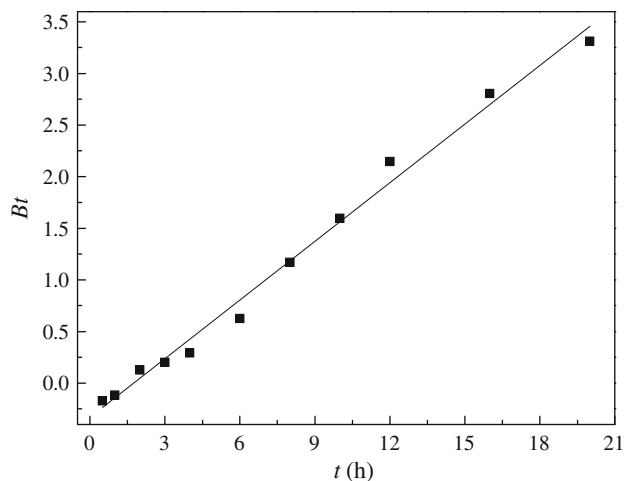**Fig. 11** Weber–Morris plots for cesium adsorption on PAN-KNiCF

Fig. 12 Bt versus t plot for cesium adsorption onto PAN-KNiCF

Table 3 Weber–Morris and Boyd model parameters for the sorption of cesium

Weber–Morris model				Boyd model	
k_i (mg/ (g h$^{0.5}$))	$D_i \times 10^8$ (m^2/h)	I (mg/g)	R^2	$D_{eff} \times 10^9$ (m^2/h)	R^2
22.868	2.760	16.974	0.955	9.400	0.990

In addition, intraparticle diffusion coefficient can be calculated from intraparticle diffusion rate constant by the following equation:

$$D_i = \frac{5\pi}{12} \left(\frac{d_p k_i}{q_e} \right)^2 \tag{6}$$

where D_i (m^2/h) is the intraparticle diffusion coefficient, d_p (m) is particle diameter. The parameters related to Weber–Morris model are summarized in Table 3.

To determine the actual rate limiting step of adsorption process, the adsorption data were further analyzed by the Boyd model, which is presented by the following equations [16]:

$$F = \frac{q_t}{q_e} \tag{7}$$

and

$$F = 1 - \frac{6}{\pi^2} \exp(-Bt), \tag{8}$$

i.e.

$$Bt = -0.4977 - \ln(1 - F), \tag{9}$$

where F is the fractional attainment of equilibrium at time t and Bt is a mathematical function of F.

The value of Bt can be calculated from each value of F and the values are plotted against t as shown in Fig. 12.

The linearity of this plot can be used to distinguish between film diffusion and intraparticle diffusion mechanism [19]. From Fig. 12, it was observed that the plot were linear but did not pass through the origin, indicating that, for the studied solute concentration, film diffusion mainly governs the rate-limiting process [20].

The calculated B value was used to calculate the effective diffusion coefficient by the following equation [21]:

$$B = \frac{\pi^2 D_{eff}}{r^2} \tag{10}$$

where D_{eff} (m^2/h) is the effective diffusion coefficient of sorbates in the adsorbent phase and r (m) is the radius of adsorbent particle.

Adsorption isotherms

The adsorption of Cs$^+$ on the adsorbent at different concentrations was investigated at constant temperature, i.e., 303 K. The results obtained are shown in Fig. 13. The amount of cesium taken by PAN-KNiCF exhibited a fast initial increase followed by a slight increase with increasing adsorptive concentration.

Langmuir, Freundlich and Dubinin-Radushkevich models were applied to further analyze adsorption data in order to reveal the equilibrium relationship between the concentration in the aqueous phase and the concentration in the adsorbent particles.

The Langmuir isotherm is one of the simplest and most useful isotherm models proposed by Langmuir. The isotherm is valid for monolayer adsorption onto a surface containing a finite number of identical sites. The Langmuir equation is of the form [22]:
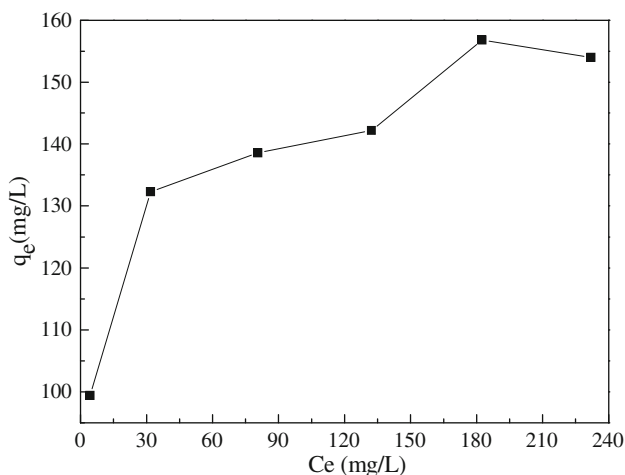
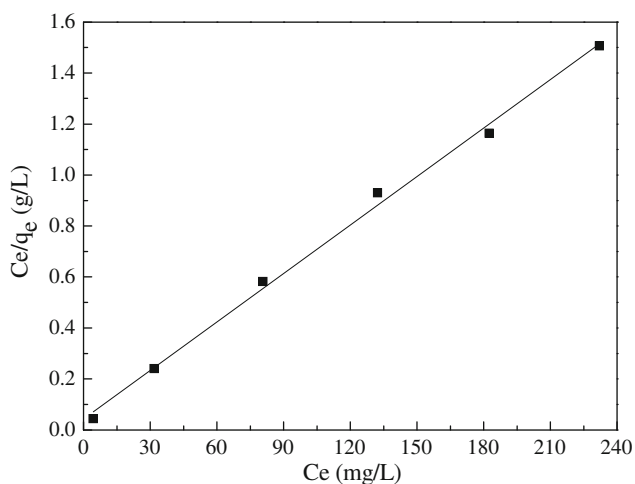**Fig. 13** Experimental adsorption isotherm of cesium on the PAN-KNiCF at 303 K

Table 4 Langmuir, Freundlich and Dubinin-Radushkevich model parameters for cesium adsorption isotherms at 303 K

Langmuir isotherm	Q_0 (mg/g)	157.729
	K_L (L/mg)	0.146
	R^2	0.996
Freundlich isotherm	K_F (mg/g)(L/mg)$^{1/n}$	86.391
	n	9.164
	R^2	0.954
Dubinin-Radushkevich isotherm	K_D (kJ^2/mol^2)	0.00103
	q_m (mol/g)	0.00152
	E (kJ/mol)	22.033
	R^2	0.965

Fig. 14 Langmuir adsorption isotherm of cesium on PAN-KNiCF at 303 K
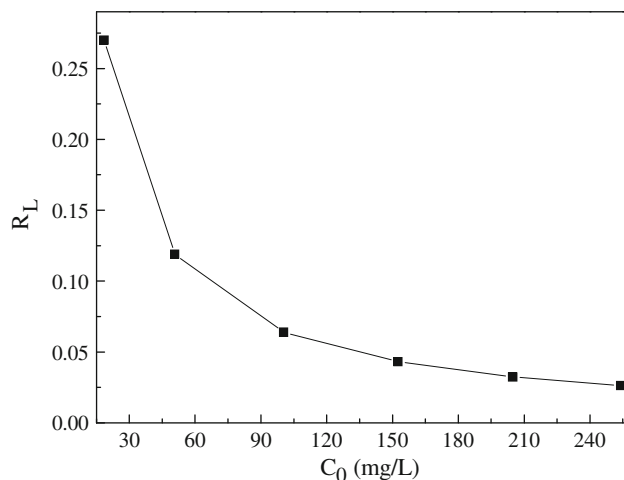
Fig. 15 Separation factor R_L of cesium on PAN-KNiCF

$$\frac{C_e}{q_e} = \frac{1}{Q_0 K_L} + \frac{C_e}{Q_0} \tag{11}$$

where q_e (mg/g) is equilibrium solid phase sorbate concentration, C_e (mg/L) is equilibrium aqueous phase sorbate concentration, Q_0 (mg/g) is asymptotic maximum solid phase sorbate concentration, K_L is equilibrium constant (L/mg). A plot of C_e/q_e versus C_e would result in a straight line with a slope of $1/Q_0$ and intercept of $1/Q_0 K_L$ as seen in Fig. 14. Langmuir parameters are given in Table 4.

The affinity between the sorbate and sorbent can be predicted by the Langmuir parameters using the dimensionless separation factor R_L:

$$R_L = \frac{1}{1 + K_L C_0} \tag{12}$$

where K_L is equilibrium constant and C_0 is initial concentration of the sorbate in solution.

The values of R_L indicate the type of isotherm to be irreversible ($R_L = 0$), favorable ($0 < R_L < 1$), linear ($R_L = 1$) or unfavorable ($R_L > 1$). The calculated R_L values versus initial cesium concentration were represented in Fig. 15. From this figure, it was observed that values of R_L were in the range of 0–1 at all initial cesium concentrations and adsorption of cesium was found more favorable at higher concentrations.

Freundlich isotherm model allows for several kinds of sorption sites on the solid and represents properly the sorption data at low and intermediate concentrations on heterogeneous surfaces. The model is given by the following equation [23]:

$$\log q_e = \log K_F + \frac{1}{n}\log C_e \tag{13}$$

where K_F represents the sorption capacity when sorbate equilibrium concentration equals to 1. $1/n$ represents the
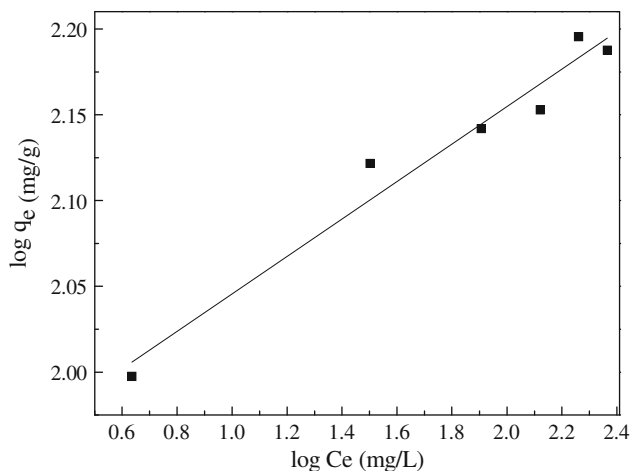
Fig. 16 Freundlich adsorption isotherm of cesium on PAN-KNiCF at 303 K

Fig. 17 Dubinin-Radushkevich adsorption isotherm of cesium on PAN-KNiCF at 303 K

degree of dependence of sorption with equilibrium concentration and n is a measure of the deviation from linearity of adsorption. A plot of log q_e versus log C_e would result in a straight line with a slope of $1/n$ and intercept of log K_F as seen in Fig. 16. Freundlich parameters are given in Table 4.

The Dubinin-Radushkevich isotherm does not assume a homogeneous surface or constant sorption potential and is more general than the Langmuir isotherm. The Dubinin-Radushkevich model is given by the equation [24]:

$$\ln q_e = \ln q_m - K_D \varepsilon^2 \tag{14}$$

where q_e (mol/g) is equilibrium solid phase sorbate concentration, q_m (mol/g) is the theoretical saturation capacity, K_D (mol^2/kJ^2) is Dubinin-Radushkevich model constant, and ε is the Polanyi potential which is in the form of:

$$\varepsilon = RT \ln\left(1 + \frac{1}{C_e}\right) \tag{15}$$

where R (8.314 J/(mol K)) is the gas constant, C_e (mol/g) is equilibrium aqueous phase sorbate concentration and T is the absolute temperature (K).

The values of q_m and K_D can be obtained by plotting ln q_e versus ε^2 (Fig. 17). The K_D is related to the adsorption energy, E (kJ/mol), which may be calculated by the following equation:

$$E = \frac{1}{\sqrt{2K_D}} \tag{16}$$

The values of q_m, K_D and E are given in Table 4.

From a comparison of the correlation coefficient values of Freundlich, Langmuir, and Dubinin–Radushkevich models, it can be concluded that Langmuir model is the most suitable and the adsorption of cesium on the PAN-
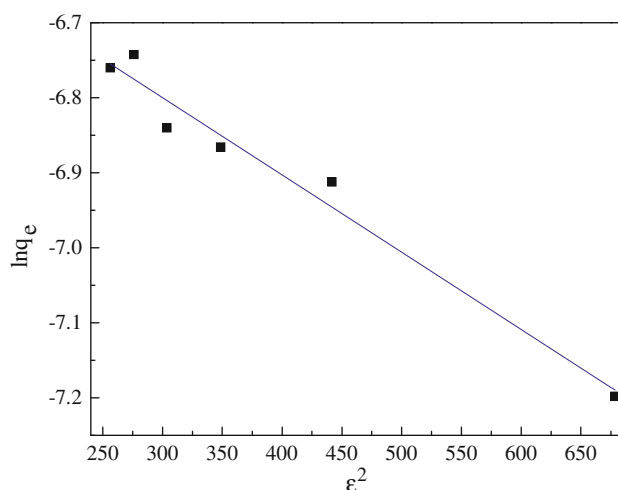
KNiCF is monolayer over the entire range of adsorptive concentration studied. The maximum exchange capacity is approximate to 1.19 mmol/g, which suggests that only about 1.19 mmol K$^+$ associated with KNiCF is exchangeable for a gram of PAN-KNiCF.

Column experiments

Generally, breakthrough curve is used to describe the performance of packed beds. The breakthrough curve shows the loading behavior of cesium to be removed from solution in a fixed bed and is usually defined as the ratio of effluent cesium concentration to influent cesium concentration (C/C_0) as a function of time or volume of effluent for a given bed height. Moreover, the Thomas model was used to further analyze data obtained from column experiments in order to predict the breakthrough curves and to determine maximum adsorption capacity and column kinetic parameters.

The Thomas model has the following form [25]:

$$\frac{C}{C_0} = \frac{1}{1 + \exp\left(\frac{k_{Th}}{v}(q_0 M - C_0 V)\right)} \tag{17}$$

where C_0 and C are cesium ion concentrations (mg/L) in the influent and effluent, respectively, k_{Th} (mL/(min mg)) is the Thomas rate constant, v (mL/min) is the flow rate, q_0 (mg/g) is the maximum adsorption capacity, M (g) is the amount of adsorbent in the column and V (L) is the volume of metal solution passed through the column.

Experimental and Thomas model breakthrough curves for flow rate of 1 and 3 BV/min were given in Figs. 18 and 19. The kinetic coefficient k_{Th} and the maximum adsorption capacity q_0 given in Table 5 were determined from Thomas model breakthrough curves.
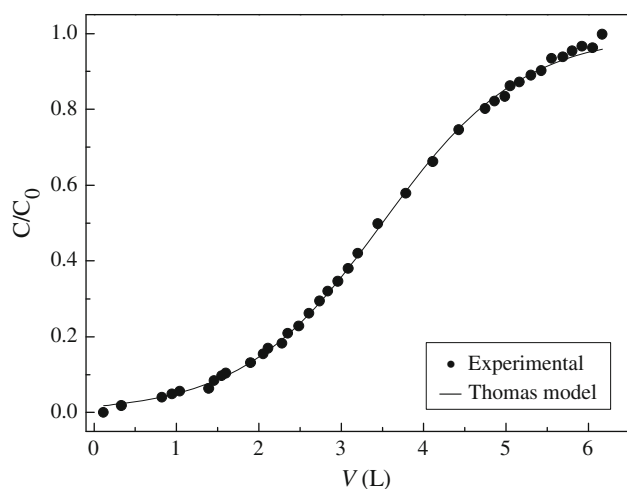
Fig. 18 Experimental and Thomas model breakthrough curves for flow rate of 1 BV/min
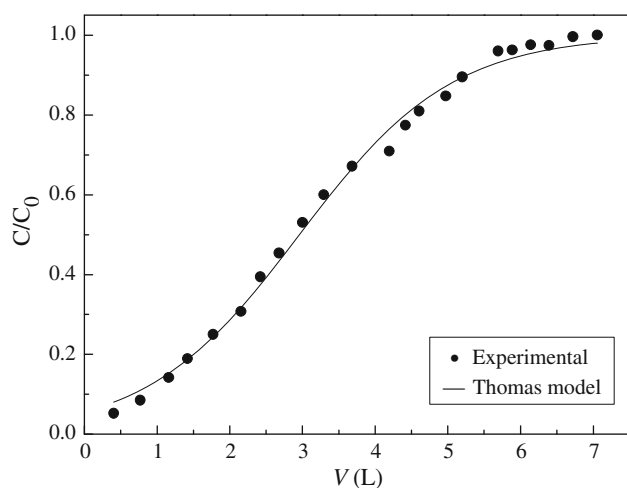

Fig. 19 Experimental and Thomas model breakthrough curves for flow rate of 3 BV/min

Table 5 Thomas model parameters for adsorption of cesium on PAN-KNiCF

1 BV/min			3 BV/min		
k_{Th} (mL/ (min mg))	q_0 (mg/g)	R^2	k_{Th} (mL/ (min mg))	q_0 (mg/g)	R^2
0.130	139.925	0.999	0.312	119.539	0.995

The Thomas model parameters are given in Table 5. The Thomas model gave a good fit of the experimental data, at both the flow rates examined, with correlation coefficients greater than 0.990, which would indicate that the external and internal diffusions were not the rate limiting step [26]. The maximum adsorption capacity (q_0) decreased with increasing flow rate. However, the rate constant (k_{Th}) increased with increasing flow rate which indicates that the mass transport resistance decreases. The

reason is that the driving force for adsorption is the cesium concentration difference between PAN-KNiCF and solution.

Conclusion

The experimental findings in this work showed that the synthesized composite have crystalline structure and KNiCF have a chemical formulation of $K_{1.16}Ni_{1.37}[Fe(CN)_6] \cdot nH_2O$. The batch experiments showed that the adsorption of cesium is directly depended upon the contact time, solution initial pH, other cations and initial cesium concentration. The PAN-KNiCF showed high selectivity for cesium removal and the order of K_d of cesium in the presence of coexisting ions up to 100 mg/L concentration was found to be $Na^+ > Mg^{2+} > Ca^{2+} > K^+ > NH_4^+$. The equilibrium data obtained in this study accorded excellently with the Langmuir adsorption isotherm and pseudo-second-order kinetic model over the entire concentration range investigated. From the equilibrium data, it can be also concluded that film diffusion mainly governs the rate-limiting process. The overall results indicate the possibility of using the synthesized composite for efficient removal of cesium from aqueous solutions. Furthermore, its spherical shape allows it to be used successfully in column separation processes. Complete breakthrough curves were generated at feed rate of 1 and 3 BV/min and sorbent capacities were determined to be approximately 139.925 and 119.539 mg Cs/g PAN-KNiCF, respectively.

References

1. Tranter TJ, Herbst RS, Todd TA, Olson AL, Eldredge HB (2002) Evaluation of ammonium molybdophosphate-polyacrylonitrile (AMP-PAN) as a cesium selective sorbent for the removal of ^{137}Cs from acidic nuclear waste solutions. Adv Environ Res 6:107–121
2. Marinin DV, Brown GN (2000) Studies of sorbent/ion-exchange materials for the removal of radioactive strontium from liquid radioactive waste and high hardness groundwaters. Waste Manage (Oxford) 20:545–553
3. Mishra SP, Tiwari D, Prasad SK, Dubey RS, Mishra M (2006) Inorganic ion-exchangers in radioactive waste management Part XVI: uptake of some metal phosphates (stannic and zirconium) for ^{134}Cs. J Radioanal Nucl Chem 268(2):191–199
4. Mimura H, Lehto J, Harjula R (1997) Ion exchange of cesium on potassium nickel hexacyanoferrate(II)s. J Nucl Sci Technol 34(5):484–489
5. Loos-Neskovic C, Ayrault S, Badillo V, Jimenez B, Garnier E, Fedoroff M, Jones DJ, Merinov B (2008) Structure of copper-potassium hexacyanoferrate(II) and sorption mechanism of cesium. J Solid State Chem 177:1817–1828
6. Orechovská J, Rajec P (1999) Sorption of cesium on composite sorbents based on nickel ferrocyanide. J Radioanal Nucl Chem 242(2):387–390

7. Saberi R, Nilchi A, Garmarodi SR, Zarghami R (2010) Adsorption characteristic of ^{137}Cs from aqueous solution using PAN-based sodium titanosilicate composite. J Radioanal Nucl Chem 284:461–469

8. Nilchi A, Atashi H, Javid AH, Saberi R (2007) Preparation of PAN-based adsorbers for separation of cesium and cobalt from radioactive wastes. Appl Radiat Isot 65:482–487

9. Motl A, John J, Sebesta F (1997) Composite absorbers of inorganic ion-exchangers and polyacrylonitrile binding matrix V. Influence of ionizing radiation on the leachability of ^{137}Cs from cemented composite NiFC-PAN absorber. J Radioanal Nucl Chem 222(1):205–207

10. Someda HH, ElZahhar AA, Shehata MK, El-Naggar HA (2002) Supporting of some ferrocyanides on polyacrylonitrile (PAN) biding polymer and their application for cesium treatment. Sep Purif Technol 29:53–61

11. Moon JK, Kim KW, Jung CH, Shul YG, Lee EH (2000) Preparation of organic-inorganic composite adsorbent beads for removal of radionuclides and heavy metal ions. J Radioanal Nucl Chem 246:299–307

12. Kalavathy MH, Karthikeyan T, Rajgopal S, Miranda LR (2005) Kinetic and isotherm studies of Cu(II) adsorption onto H$_3$PO$_4$-activated rubber wood sawdust. J Colloid Interf Sci 292:354–362

13. Lagergren S (1898) About the theory of so-called adsorption of soluble substances. Kungliga Svenska Vetenskapsakademiens, Handlingar 24(4):1–39

14. Ho YS, McKay G (1999) Pseudo-second order model for sorption processes. Process Biochem 34(5):451–465

15. Kumar KV, Ramamurthi V, Sivanesan S (2005) Modeling the mechanism involved during the sorption of methylene blue onto fly ash. J Colloid Interf Sci 284:14–21

16. Sarkar M, Acharya PK, Bhattacharya B (2003) Modeling the adsorption kinetics of some priority organic pollutants in water from diffusion and activation energy parameters. J Colloid Interf Sci 266:28–32

17. Svilović S, Rušić D, Bašić A (2010) Investigations of different kinetic models of copper ions sorption on zeolite 13. Desalination 259:71–75

18. Chen H, Zhao Y, Wang A (2007) Removal of Cu(II) from aqueous solution by adsorption onto acid-actived palygorskite. J Hazard Mater 149:346–354

19. Wang S, Li H, Xu L (2006) Application of zeolite MCM-22 for basic dye removal from wastewater. J Colloid Interf Sci 295(1):71–78

20. Kumar KV, Ramamurthi V, Sivanesan S (2005) Modeling the mechanism involved during the sorption of methylene blue onto fly ash. J Colloid Interf Sci 284:14–21

21. Naveen N, Saravanan P, Baskar G, Renganathan S (2011) Equilibrium and kinetic modeling on the removal of Reactive Red 120 using positively charged Hydrilla verticillata. J Taiwan Inst Chem E 42:463–469

22. Langmuir I (1916) The constitution and fundamental properties of solids and liquids. J Am Chem Soc 38:2221–2295

23. Freundlich HMF (1906) Uber die adsorption in losungen. J Phys Chem 57:385–470

24. Mellah A, Chegrouche S, Barkat M (2006) The removal of uranium(VI) from aqueous solutions onto activated carbon: kinetic and thermodynamic investigations. J Colloid Interf Sci 296:434–441

25. Öztürk N, Kavak D (2005) Adsorption of boron from aqueous solutions using fly ash: batch and column studies. J Hazard Mater B127:81–88

26. Aksu Z, Gonen F (2004) Bisorption of phenol by immobilized activated sludge in a continuous packed bed: prediction of breakthrough curves. Process Biochem 39:599–613